Hindawi
Advances in Civil Engineering
Volume 2021, Article ID 5565320, 8 pages
https://doi.org/10.1155/2021/5565320

Research Article

The Analysis of Anchoring Mechanism of Rock Slope in Two Layers Based on the Nonlinear Twin-Shear Strength Criterion

X. B. Gu,[1] **Y. H. Wang**,[2] **X. J. Ji**,[1] **and Y. H. Zhu**[3]

[1]*School of Civil Engineering, Nanyang Institute of Technology, Nanyang, China*
[2]*School of Civil Engineering, Sichuan University of Science & Engineering, Zigong, China*
[3]*School of Civil Engineering, Neijiang Normal University, Neijiang, Sichuan, China*

Correspondence should be addressed to X. J. Ji; jifeng988@163.com

Received 18 February 2021; Revised 11 March 2021; Accepted 28 March 2021; Published 3 May 2021

Academic Editor: Yunteng Wang

The nonlinear strength criterion is introduced into the paper firstly, and then the geometric anchoring characteristic model of rock slope separated from two layers according to rock type with the fracture surface of log-spiral curve considering nonlinear twin-shear criterion subjected to seismic loads is established. Finally, some correlated influential parameters are analyzed, and the conclusions are drawn, showing that the intermediate principal stress has great influence on the total anchoring force of bolt P, so when different criteria are selected, the influence of intermediate principal stress should not be omitted. The effects of thickness ratio h_1/h_2 on total anchoring force increase gradually with the increase of inclination angle ϕ. The total anchoring force P decreases gradually with the increase of inclination angle ϕ and surcharge load q. The total anchoring force increases gradually with the increase of horizontal seismic acceleration coefficients k_h and geometric coefficients m_i and GSI.

1. Introduction

The destabilization of slope is a complex and dangerous geological disaster phenomenon [1]; it brings about huge harms to the safety of life and property, so the investigation on the slope stability is always focused on [2–4]. Many supporting schemes are adopted in the process of slope governance, for example, antislide pile and retaining wall. Meanwhile, their many shortcomings are found in the application of civil engineering [5], such as high cost, difficult construction, and heavy work. To overcome the mentioned problems [6], the application of the anchoring bar on the slope solves the above problem, and anchoring bar plays a great role in the support of slope [7]. So, a great deal of theoretical and experimental investigations about the supporting theory of anchoring bar are performed. The mechanical mechanism of the load transfer of anchoring bar is studied by Lutz et al. [8–10]. The influential factors about the bearing capacity of anchoring bar are analyzed by Hyet and Badwen [11] using a great deal of experimental investigations. In China, the further investigation about the anchoring technology in the geotechnical engineering is performed. The fracture modes of foundation pit with the support of anchoring bar are investigated by Jin-Qing and Zheng [12] using the limit equilibrium theory and finite difference method. Then, the optimum design of mechanical model is calculated by Li-De and Cong-Xin [13] by using the strength reduction method of finite element. The distribution law of loads along the anchoring bar and the mechanism of anchoring forces are studied by Gamse and Oberguggenberger [14] by using numerical simulation and theoretical investigation. Then, the consolidation actions of anchoring bar on the layer rock slope are simulated by Chen et al. [15] using the finite difference software FLAC3D. To investigate the anchoring mechanism of rock slope, lots of fracture criteria are utilized [16]; for example, Mohr–Coulomb criterion [17] and Hoek–Brown criterion [18] are often adopted; although the obvious effects are obtained in the actual engineering, the influences of intermediate principal stress in these criteria are often omitted [19, 20], and a large deal of engineering practices demonstrated that the influence of intermediate principal stress

should be valued [21], so the twin-shear strength criterion in the paper is introduced; and, to conform to the engineering practice, earthquake loads, different rock types, and fracture modes of rock slope are, respectively, considered in the paper, a new thought and method for the stability design of rock slope can be provided.

The paper is organized as follows. In Section 2, nonlinear twin-shear criteria and method of upper bound limit analysis are introduced at first. In Section 3, the mechanical model of rock slope with the anchoring bar is established, the kinematic method of limit analysis considering nonlinear twin-shear criteria is deduced, and the anchoring mechanism of rock slope is analyzed. In Section 4, results and discussions are performed. In Section 5, conclusions are drawn.

2. Method and Theory

2.1. The Relevant Fracture Criterion. The nonlinear united strength failure criterion can be expressed as [22]

$$F = \sigma_1 - \frac{1}{1+c}\left(c\sigma_2 + \sigma_3\right) - \sigma_c\left[\frac{m}{(1+c)\sigma_c}\left(c\sigma_2 + \sigma_3\right) + s\right]^{(1/2)} = 0, \quad \text{when } F \geq F', \tag{1}$$

$$F^{'} = \frac{1}{1+b}\left(\sigma_1 + c\sigma_2\right) - \sigma_3 - \sigma_c\sqrt{\frac{m\sigma_3}{\sigma_c} + s} \leq 0, \quad \text{when } F < F', \tag{2}$$

where σ_c is the uniaxial compressive strength of intact rock, m is constant value, and b represents the intermediate principle stress coefficients; s is a constant value relevant to the rock mass and it can be determined in the two following equations:

$$\frac{m}{m_i} = \exp\left(\frac{\mathrm{GSI} - 100}{28 - 14\ D}\right), \tag{3}$$

$$s = \exp\left(\frac{\mathrm{GSI} - 100}{9 - 3\ D}\right), \tag{4}$$

where D is a disturbance coefficient, and its range is from 0.0 to 1.0.GSI is the geological strength index, and its range is from 0 to 80. The magnitude of m_i is obtained from compression tests on an intact rock. If no test data are available, Hoek parents the approximate values for five types of rocks as follows [23]:

(1) When the value of $m_i \approx 7$, it is applied to calculate carbonate rock types, such as dolomite, limestone, and marble

(2) When the value of $m_i \approx 10$, it is applied to calculate lithified argillaceous rock types, such as mudstone, siltstone shale, and slate

(3) When the value of $m_i \approx 15$, it is applied to calculate arenaceous rock types, such as mudstone, siltstone shale, and slate

(4) When the value of $m_i \approx 17$, it is applied to calculate fine-grained polymineralic igneous crystalline rock types, such as andesite, dolerite, and diabase

(5) When the value of $m_i \approx 25$, it is applied to calculate coarse-grained polymineralic igneous and metamorphic rock types, such as amphibolite, gabbro, gneiss, granite, and quartz diorite

In equations (1) and (2), when $c = 0$, this demonstrates that the influences of the intermediate principal stress are omitted, so Hoek–Brown criterion can be expressed as follows:

$$F = \sigma_1 - \sigma_3 - \sigma_c\left[\frac{m\sigma_3}{\sigma_c} + s\right]^{(1/2)}. \tag{5}$$

For $c = 1$, this demonstrates that the influences of the intermediate principal stress are taken into consideration, and the nonlinear united strength criterion can be obtained as follows [24]:

$$F(\underline{\sigma}) = \sigma_1 - \frac{1}{2}\left(\sigma_1 + \sigma_2\right) - \sqrt{\frac{m\sigma_c}{2} \times \left(\sigma_2 + \sigma_3\right) + s\sigma_c^2} \leq 0, \quad \text{when } F > F',$$

$$F(\underline{\sigma}) = \frac{1}{2}\left(\sigma_1 + \sigma_2\right) - \sigma_3 - \sqrt{m\sigma_c\sigma_3 + s\sigma_c^2} \leq 0, \quad \text{when } F < F'. \tag{6}$$

2.2. Kinematic Method of Limit Analysis. The seismic stability analysis is performed within the framework of limit analysis theory [25]. To get the upper bound solution, the construction of velocity is required in the method. The implementation of the kinematic method of limit analysis depends on the following fundamental inequality [26]:

$$\Theta_{ex}(\underline{U}) \leq \Theta_{mr}(\underline{U}), \tag{7}$$

where $\underline{U}$ is any virtual admissible velocity field. $\Theta_{ex}(\underline{U})$ is the work performed by external loading, and $\Theta_{mr}(\underline{U})$ is the maximum resisting work originating from the rock materials. The formula of maximum resisting work according to Saada's work [27] can be obtained as

$$\Theta_{mr}(\underline{U}) = \int_{\Omega} \psi\left[\underline{\underline{d}}(\underline{x})\right]\mathrm{d}\Omega + \int_{\Sigma} \psi\{\underline{\nu}(\underline{x}); [\underline{U}(\underline{x})]\}\mathrm{d}\Sigma, \tag{8}$$

where $\underline{\underline{d}}$ is the strain rate sensor associated with $\underline{U}$ at any point of rock mass volume Ω. $[\underline{U}(\underline{x})]$ means the jump at a point $\underline{x}$ through a possible velocity discontinuity surface Σ and $\Sigma\prime$ following its normal $\underline{\nu}(\underline{x})$, and the ψ-functions are the support functions defined by the duality from the strength condition $F(\underline{\underline{\sigma}}) \leq 0$.

$$\psi\left[\underline{\underline{d}}\right] = \sup_{\underline{\underline{\sigma}}}\left\{\underline{\underline{\sigma}} : \underline{\underline{d}} \,|F(\sigma) \leq 0\right\}, \tag{9}$$

$$\psi\left[\nu; [\underline{U}]\right] = \sup_{\underline{\underline{\sigma}}}\left\{[\underline{U}] \cdot \underline{\underline{\sigma}} \cdot \underline{\nu} \,|F(\sigma) \leq 0\right\}. \tag{10}$$

For nonlinear twin-shear rock masses, the corresponding 3D closed-form expressions of the foregoing ψ-functions are obtained as follows [28]:

$$\psi\left[\underline{\underline{d}}\right] = -\frac{s\sigma_c}{m} tr\,\underline{\underline{d}} + \frac{3}{4} m\sigma_c \frac{\chi\left(\underline{\underline{d}}\right)}{\mathrm{tr}\,\underline{\underline{d}}}, \quad \text{if } \mathrm{tr}\,\underline{\underline{d}} \geq 0, \tag{11}$$

$$\chi\left(\underline{\underline{d}}\right) = \left[\max\left(0, d_1\right) + \max\left(0, d_2\right) + \max\left(0, d_3\right)\right]^2, \tag{12}$$

where d_1, d_2, and $d_3$represent the eigenvalues of $\underline{\underline{d}}$.

Similarly, it has been found that the ψ-functions relative to a velocity jump and defined by equation (7) take the following form:

$$\psi\left[\underline{v}; [\underline{U}]\right] = -\frac{s\sigma_c}{m} [\underline{U}] \cdot \underline{v} + \frac{3}{4} m\sigma_c \frac{\chi\left(\underline{v}; [\underline{U}]\right)}{[\underline{U}] \cdot \underline{v}}, \quad \text{if } [\underline{U}] \cdot \underline{v} > 0, \tag{13}$$

where

$$\chi\left(\underline{v}; [\underline{U}]\right) = \frac{1}{4}\left(\left|[\underline{U}]\right| - [\underline{U}] \cdot \underline{v}\right)^2. \tag{14}$$

It should be noted that the conditions $\mathrm{tr}\,\underline{\underline{d}} > 0$ in equation (11) and $[\underline{U}] \cdot \underline{v} > 0$ in equation (13) demonstrate the fact that $\psi[\underline{\underline{d}}] < +\infty$ and $\psi[\underline{v}; [\underline{U}]] < +\infty$, respectively. These conditions are necessary for the kinematic method of limit analysis expressed by equation (7) which results in nontrivial upper bound solutions.

3. The Establishment of Mechanical Model

3.1. The Analysis of Failure Mechanism. The failure mechanism, depicted in Figure 1 and considered in the investigation, is a direct transportation of those usually employed for homogeneous nonlinear twin-shear strengthen slope. In such model, two layers of rock mass are composed in the rock mass slope, there are, respectively, different compressive strengths and unit weight in two layers, and the earthquake loads are considered in two layers of rock mass; and the quasistatic method is adopted in the manuscript. Because horizontal wave has a great influence on the fracture of rock slope, only horizontal action of earthquake loads is considered. Its inclined angle along the fracture surface AC is ϕ. The failure routine is a straight line in the upper layers of rock slope, and it is assumed that the fracture surface is parallel with the rock slope surface, so quadrangle is parallel quadrangle. There exist uniform distribution external loads q in the roof of rock slope. There are lots of support bars in the rock slope surface. It is assumed that fracture surface of rock slope represents a log-spiral curve in lower layer of rock slope, a volume of rock mass is rotating about a point O with an angular velocity ω, the curve CE separating this volume from the structure that is kept motionless is a log-spiral arc and focus O, and it necessarily follows that the velocity jump at any point of line CE is inclined at angle ϕ with respect to the tangent at the same point. The inclination angle of anchoring bar is β with a horizontal direction. Five parameters are involved in such a mechanism: four angles θ_1, θ_2, ϕ, and β and the distance $r_0 = R$ defining the radius of log-spiral curve for $\theta = \theta_1$; accordingly, this curve is defined in polar coordinates (o, r, θ) by equation $r = r_0 e^{(\theta - \theta_1)\tan\phi}$.

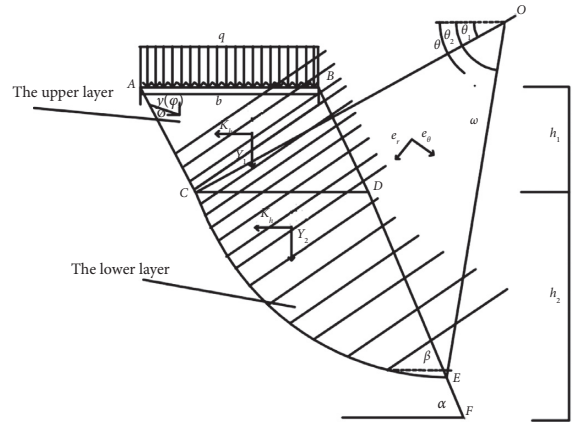

Figure 1: The anchoring mechanism of rock slope.

3.2. The Work Rate of External Forces and Maximum Resisting Work Rate

3.2.1. The Work of External Forces in the Upper Layer of Rock Slope

(1) The work rate of gravitational force is

$$\Theta_{ug} = \gamma_1 b h_1 V \sin(\beta - \phi), \tag{15}$$

where Θ_{ug} is the work rate of gravitational force in the upper layer of rock slope; γ_1 is the unit weight of rock mass in the upper layer of rock slope.

(2) The work rate of external load q is

$$\Theta_{uq} = qbV \sin(\beta - \phi), \tag{16}$$

where Θ_{uq} is the work rate of uniform distribution load q and b is the width of roof.

(3) The work rate of seismic load is

$$\Theta_{uhs} = -k_h \gamma_1 b h_1 V \cos(\beta - \phi), \tag{17}$$

where Θ_{uhs} is the work rate of horizontal earthquake loads in the upper layer; k_h is the horizontal earthquake load coefficient.

(4) The work rate of roof bolt is

$$\Theta_{up} = -\sum_{i=1}^{n} P_i V \cos(\beta - \phi)\cos\beta, \tag{18}$$

where Θ_{up} is the work rate of antisliding force about anchors in the upper layer; P_i is the antisliding force of the ith roof bolt.

(5) The maximum resisting work rate is

$$\Theta_{mru} = \sigma_{Cu} \frac{h_1}{\sin\alpha} V \cos\phi \left[-\frac{s}{m} + \frac{3}{4} m \left(\frac{1 - \sin\phi}{2\sin\phi}\right)^2\right], \tag{19}$$

where Θ_{mru} is the maximum resisting work rate in the upper layer; σ_{Cu} is the compressive strength of rock mass in the upper layer.

3.2.2. The Work Rate of External Forces in the Lower Layer of Rock Slope

(1) The work rate of gravitational force is

$$\Theta_{\mathrm{lg}} = \gamma_2 r_0^3 \omega (l_1 + l_2 + l_3), \tag{20}$$

where Θ_{lg} is the work of gravitational force; expressions of l_1, l_2, and l_3 can be, respectively, expressed as

$$l_1 = \frac{1}{3}\frac{e^{3\tan\varphi(\theta_1-\theta_2)}(3\tan\varphi\cos\theta_2+\sin\theta_2)-(3\tan\varphi\cos\theta_1+\sin\theta_1)}{9\tan^2\varphi+1}, \tag{20a}$$

$$l_2 = \frac{1}{6}\sin\theta_1\left[\frac{2b}{r_0}\cos\theta_1-\left(\frac{b}{r_0}\right)^2\right], \tag{20b}$$

$$l_3 = -\frac{1}{3}\left(\frac{r_B}{r_0}\right)^3\sin^3(\theta_B+\alpha)\left[\frac{\cos\alpha}{2}\left(\frac{1}{\sin^2(\theta_B+\alpha)}-\frac{1}{\sin^2(\theta_2+\alpha)}\right)+\sin\alpha\left(\frac{\cos(\theta_B+\alpha)}{\sin(\theta_B+\alpha)}\frac{\cos(\theta_2+\alpha)}{\sin(\theta_2+\alpha)}\right)\right]. \tag{20c}$$

(2) The work rate of seismic load is

$$\Theta_{\mathrm{lhs}} = k_h \gamma_2 r_0^3 \omega (l_4 + l_5 + l_6), \tag{21}$$

where Θ_{lhs} is the work rate of seismic load. The expressions of l_4, l_5, and l_6 can be, respectively, expressed as

$$l_4 = \frac{1}{3}\frac{e^{\tan\varphi(\theta_1-\theta_2)}(3\tan\varphi\cos\theta_2-\cos\theta_2)-(3\tan\varphi\sin\theta_1-\cos\theta_1)}{9\tan^2\varphi+1}, \tag{21a}$$

$$l_5 = -\frac{1}{3}\left(\frac{b}{r_0}\right)\sin^3\theta_1, \tag{21b}$$

$$l_6 = -\frac{1}{3}\left(\frac{r_B}{r_0}\right)^3\sin^3(\theta_B+\alpha)\left[-\frac{\sin\alpha}{2}\left(\frac{1}{\sin^2(\theta_B+\alpha)}-\frac{1}{\sin^2(\theta_2+\alpha)}\right)+\cos\alpha\left(\frac{\cos(\theta_B+\alpha)}{\sin(\theta_B+\alpha)}\frac{\cos(\theta_2+\alpha)}{\sin(\theta_2+\alpha)}\right)\right], \tag{21c}$$

where different parameters are shown in formulas (20)–(21c). The expressions of r_B and θ_B can be, respectively, expressed as

$$r_B = r_0\sqrt{1-2\left(\frac{b}{r_0}\right)\cos\theta_1+\left(\frac{b}{r_0}\right)^2}, \tag{21d}$$

$$\theta_B = \arctan\left(\frac{\sin\theta_1}{\cos\theta_1-(b/r_0)}\right). \tag{21e}$$

(3) The work rate of roof bolt is

$$\Theta_{lp} = \sum_{i=1}^{n} P_i r_0 \omega e^{(\theta-\theta_1)\tan\phi}\sin(\theta-\beta), \tag{22}$$

where Θ_{lp} is the work rate of antislide force of roof bolts; P_i is the antisliding force of the i*th* bolt. i is the number of roof bolts.

(4) The maximum resisting work rate is defined as follows.

The maximum resisting work results from the velocity jump along the log-spiral line CF, and the expression of resisting work derived from equations (10)–(12) can be depicted as follows:

$$\Theta_{\mathrm{mrl}} = \frac{1}{2}\sigma_{CL}\omega r_0^2\left(e^{2(\theta_1-\theta_2)\tan\phi}-1\right)\left[-\frac{s}{m}+\frac{3}{4}m\left(\frac{1-\sin\phi}{2\sin\phi}\right)^2\right]. \tag{23}$$

3.2.3. The Expression of Anchoring Force. According to the fundamental inequality (7), the expression of anchoring force $\sum_{i=1}^{n} P_i$ can be shown as follows:

$$\sum_{i=1}^{n} P_i \le \frac{\Theta_{mru}+\Theta_{mrl}-\Theta_{ug}-\Theta_{uq}+\Theta_{uhs}-\Theta_{lhs}-\Theta_{\mathrm{lg}}}{r_0\omega e^{(\theta-\theta_1)\tan\phi}\sin(\theta-\beta)-V\cos(\beta-\theta)\cos\beta}. \tag{24}$$

3.2.4. The Critical Anchoring Force. According to the investigation of Ling and Leshchinsky [29], the expression of the total anchoring force is defined as

$$F = \frac{\sum_{i=1}^{n} P_i}{0.5\gamma H^2}. \tag{25}$$

According to the principal of limit analysis theory, when $f = 1$, the critical total anchoring force can be expressed as

$$F \le F_u = \min \frac{\Theta_{mru} + \Theta_{mrl} - \Theta_{ug} - \Theta_{uq} + \Theta_{uhs} - \Theta_{lhs} - \Theta_{\lg}}{0.5(h_1 + h_2)^2 \left[r_0 \omega e^{(\theta - \theta_1)\tan\phi} \sin(\theta - \beta) - V \cos(\beta - \theta)\cos\beta \right]} \left(\frac{1}{\gamma_1} + \frac{1}{\gamma_2} \right). \tag{26}$$

4. Results and Discussion

4.1. The Effects of Intermediate Principal Stress on the Total Anchoring Force. To investigate the influence of intermediate principal stress on the total anchoring force, the following parameters are listed as follows: $r_0 = 12$ m, mi = 10, GSI = 10, and $b = 5$ m; $\gamma_1 = 15\,(\mathrm{kN/m^3})$, $\gamma_2 = 20\,(\mathrm{kN/m^3})$, $h_1 = 8$ m, $h_2 = 9$ m, $q = 20$ kPa, $\omega = 0.2$, V = 0.1 mm/s, σcu = 6 MPa, σcl = 10 MPa, $\alpha = 20^\circ$, kh = 0.18, $\theta 1 = 200$, $\theta 2 = 500$, $\theta = 300$, $\theta_B = 35^\circ$, $\theta_B = 35^\circ$, and $\beta = 20^\circ$. It is shown in Figure 2 that the total anchoring force P increases as the velocity inclination angle increases whether Hoek–Brown criterion [30] or twin-shear strength criterion strengthens. However, it can be found in comparison that the magnitude for $c = 1$ (it means that the influence of intermediate principal stress is not considered) is higher than one of $c = 0$ (it means that the influence of intermediate principal stress is considered), and the conclusions are drawn, showing that the intermediate principal stress has a great influence on total anchoring force of bolt P, so when different criteria are selected, the influence of intermediate principal stress is not omitted.

4.2. The Influence of Bolt Inclination Angle on the Total Anchoring Force. The range on the inclination angle of bolt is 10–35°, so the inclination angle of anchor is, respectively, adopted for $\beta = 10^\circ$, 20°, and 30° and the comparison and analysis are carried out among three cases. The following parameters are determined: $r_0 = 12$ m, $m_i = 10$, GSI = 10, and $b = 5$ m; $\gamma_1 = 15\,(\mathrm{kN/m^3})$, $\gamma_2 = 20\,(\mathrm{kN/m^3})$, $h_1 = 8$ m, $h_2 = 9$ m, $q = 20$ kPa, $\omega = 0.2$, $V = 0.1$ mm/s, $\sigma_{cu} = 6$ MPa, $\sigma_{cl} = 10$ MPa, $\alpha = 20^\circ$, $k_h = 0.18$, $\theta_1 = 20^\circ$, $\theta_2 = 50^\circ$, $\theta = 30^\circ$, and $\theta_B = 35^\circ$. The effects of anchoring inclination angle α on the total anchoring force are depicted in Figure 3. It can be found that the total anchoring force P decreases gradually with the increase of inclined angle ϕ; and it can also be found that the total anchoring force P increases gradually as the anchoring inclination angle β increases. The influence of anchoring inclination angle β on the total anchoring force decreases gradually with the increase of velocity inclination angle ϕ. For example, for $\phi = 10^\circ$, the value of P increases approximately by 108% when the value of α increases from 10° to 30°; then, for $\phi = 15^\circ$, it increases only by 59.8%.

4.3. The Influence of Rock Layer Thickness on the Total Anchoring Force P. The effects of thickness of rock layer on the total anchoring force are depicted in Figure 4. To explain the relation, the ratio of thickness between two rock layers is, respectively, selected as 1/3, 1/2, and 2/3 in this paper, and the following parameters are listed: $r_0 = 12$ m, mi = 10, GSI = 10, and $b = 5$ m; $\gamma_1 = 15\,(\mathrm{kN/m^3})$ and $\gamma_2 = 20\,(\mathrm{kN/m^3})$; $h_1 = 8$ m; $h_2 = 9$ m; $q = 20$ kPa, $\omega = 0.2$, $V = 0.1$ mm/s, σcu = 6 MPa, σcl = 10 MPa, $\alpha = 200$, kh = 0.18, $\theta 1 = 200$, $\theta 2 = 500$, $\theta = 300$, $\theta_B = 35^\circ$, and $\beta = 20^\circ$. It can be found in Figure 4 that the total anchoring force P increases gradually as the thickness ratio of rock layer (namely, different rock types) increases, but it can be also found that the effects of thickness ratio (h_1/h_2) on total anchoring force increase gradually with the increase of inclination angle ϕ; to illustrate, for $\phi = 100$, when (h_1/h_2) increases from 1/2 to 2/3, the value of total anchoring force P increases approximately by 11.76%; then, for $\phi = 250$, when (h_1/h_2) increases from 1/2 to 2/3, the value of P increases by 27.12%. So, conclusions can be drawn, showing that the total anchoring force P increases gradually with the increase of thickness ratio, but the influence of the thickness ratio on the anchoring force P gradually increases with the increase of velocity inclination angle ϕ.

4.4. The Influence of Surcharge Load q on the Anchoring Force P. When the influence of surcharge load q is taken into account, to explain the relation, the value of surcharge load q is, respectively, adopted as 10 MPa, 15 Mpa, and 20 MPa in this paper. The following parameters are listed: $r_0 = 12$ m, mi = 10, GSI = 10, and $b = 5$ m; $\gamma_1 = 15\,(\mathrm{kN/m^3})$ and $\gamma_2 = 20\,(\mathrm{kN/m^3})$; $h_1 = 8$ m; $h_2 = 9$ m; $\omega = 0.2$, V = 0.1 mm/s, σcu = 6 MPa, σcl = 10 MPa, $\alpha = 200$, kh = 0.18, $\theta 1 = 200$, $\theta 2 = 500$, $\theta = 300$, $\theta_B = 35^\circ$, and $\beta = 20^\circ$; the effects of surcharge load q on the total anchoring force are depicted in Figure 5. It can be found that the total anchoring force P decreases gradually with the increase of inclination angle ϕ and surcharge load q. So, conclusions can be drawn, showing that the surcharge load q of rock slope has great influences on the total anchoring force P.

4.5. The Influence of Horizontal Seismic Acceleration Coefficients on the Total Anchoring Force. When the influences of horizontal seismic acceleration coefficients k_h on the

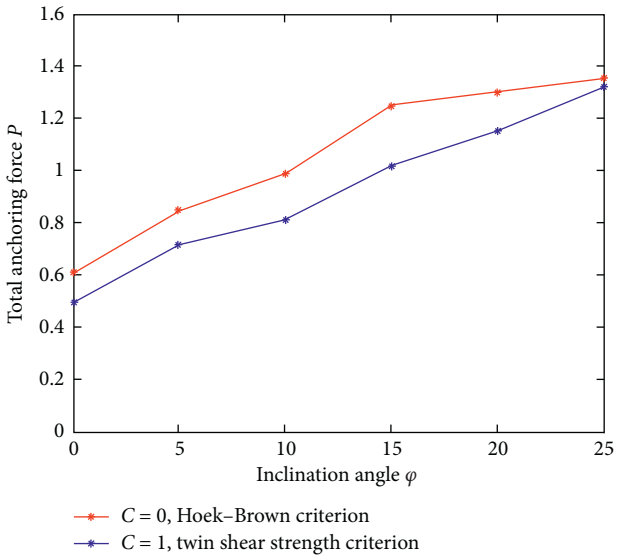

Figure 2: The relation between intermediate principal stress and anchoring force.

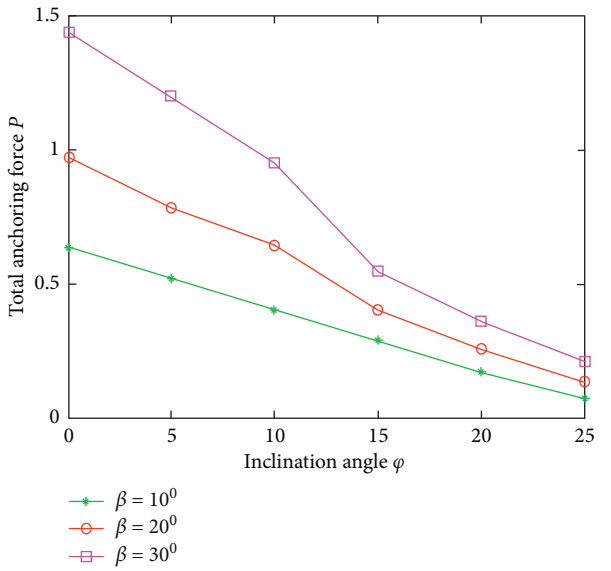

Figure 3: The relation between bolt inclination angle and anchoring force.

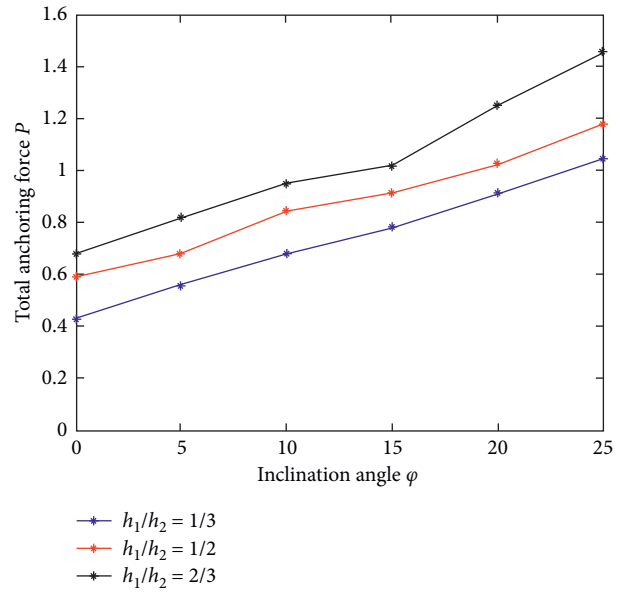

Figure 4: The relation between unit weight and anchoring force.

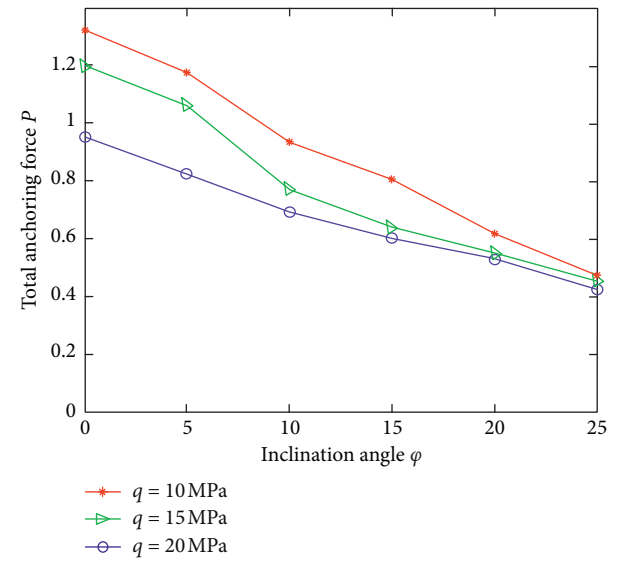

Figure 5: The relation between surcharge load and anchoring force.

anchoring force are considered, the following parameters are listed: $r_0 = 12$ m, mi = 10, GSI = 10, and $b = 5$ m; $\gamma_1 = 15\,(\mathrm{kN/m^3})$ and $\gamma_2 = 20\,(\mathrm{kN/m^3})$; $h_1 = 8$ m; $h_2 = 9$ m; $q = 30$ kPa, $\omega = 0.2$, $V = 0.1$ mm/s, σcu = 6 MPa, σcl = 10 MPa, $\alpha = 200$, $\theta 1 = 200$, $\theta 2 = 500$, $\theta = 300$, and $\theta_B = 35^0$. The effects of k_h on the total anchoring force are plotted in Figure 6. It can be found in Figure 6 that the total anchoring force increases gradually with the increase of horizontal seismic acceleration coefficients; it demonstrates that the slope becomes more dangerous; for example, for $\varphi = 100$, when the value of k_h increases from 0.08 to 0.24, the total anchoring force increases from 0.5206 to 1.0322.

4.6. The Influence of Geometric Coefficients GSI and m_i on the Total Anchoring Force. When the influences of geometric coefficients GSI and m_i on the anchoring force are, respectively, regarded, the following parameters are listed: $r_0 = 12$ m; $b = 5$ m; $\gamma_1 = 15\,(\mathrm{kN/m^3})$ and $\gamma_2 = 20\,(\mathrm{kN/m^3})$; $h_1 = 8$ m; $h_2 = 9$ m; $q = 30$ kPa, $\omega = 0.2$, $V = 0.1$ mm/s, σcu = 6 MPa, σcl = 10 MPa, $\alpha = 200$, $k_h = 0.18$, $\theta 1 = 200$, $\theta 2 = 500$, $\theta = 300$, and $\theta_B = 35°$. The effects of GSI and m_i on the anchoring force are, respectively, shown in Table 1. It can be found in Table 1 that the total anchoring force decreases gradually with the increase of geometric coefficients $m_i$and GSI, and the geometric parameters have a great influence on the total anchoring force P.

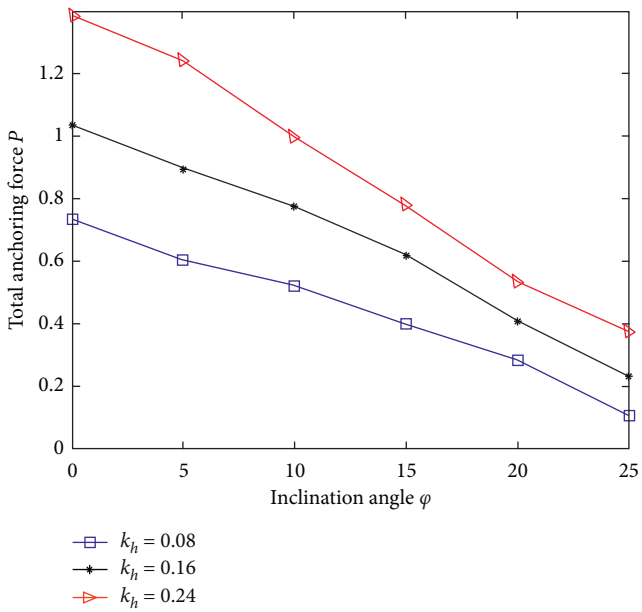

Figure 6: The relation between horizontal seismic acceleration coefficients and anchoring force.

Table 1: The relation between anchoring force P and geometric parameters GSI and m_i.

GSI	$m_i = 1$	$m_i = 10$	$m_i = 15$	$m_i = 17$	$m_i = 25$
10	1.4256	1.2826	1.0586	0.8264	0.6952
20	1.2754	1.1346	0.9421	0.7188	0.5684
30	1.1315	1.0023	0.8685	0.6021	0.5023
40	0.9524	0.8933	0.7876	0.5321	0.3956
50	0.7564	0.6992	0.6275	0.4897	0.3211
60	0.6025	0.5624	0.5033	0.4533	0.2836

5. Conclusions

The limit dynamic analysis method of upper bound solution based on nonlinear twin-shear criterion is adopted to analyze anchoring mechanism of two layers of failure slope in the investigation. The intermediate principal stress, the anchoring inclination angle β, thickness ratio (h_1/h_2) of rock layer, surcharge load q, seismic acceleration coefficients k_h, and geometric coefficients GSIand m_i have great influences on the total anchoring force. Finally, the following conclusions are drawn:

(1) The intermediate principal stress has a great influence on the total anchoring force of bolt P, so when different criteria are selected, the influence of intermediate principal stress is not omitted. The total anchoring force P decreases gradually with the increase of inclination angle ϕ. The total anchoring force P increases gradually as the anchoring inclination angle β increases. The influence of anchoring inclination angle β on the total anchoring force decreases gradually with the increase of velocity inclination angle ϕ.

(2) The total anchoring force P increases gradually as the thickness ratio of rock layer (namely, different rock types) increases. But the effects of thickness ratio (h_1/h_2) on total anchoring force increase gradually with the increase of inclination angle ϕ. The total anchoring force P decreases gradually with the increase of inclination angle ϕ and surcharge load q.

(3) The total anchoring force increases gradually with the increase of horizontal seismic acceleration coefficients. The total anchoring force decreases gradually with the increase of geometric coefficients m_i and GSI, and the geometric parameters have a great influence on the total anchoring force P.

Data Availability

The data used to support the findings of this study are available from the corresponding author upon request.

Conflicts of Interest

The authors declare that they have no conflicts of interest.

Acknowledgments

This work was supported by the first batch of Natural Science Foundation of Sichuan Provincial Department of Education (no. 17ZA0270), the cross project in Nanyang Institute of Technology (230067), the opening projection of Sichuan Province University Key Laboratory of Bridge Non-Destruction Detecting and Engineering Computing (2017QYY01), the National Natural Science Foundation of China (41672357), the Start-Up Foundation (510126), and the Sichuan Science and Technology Program (no. 2020YJ0424).

References

[1] X.-B. Gu and Q.-H. Wu, "Seismic stability analysis of waterfront rock slopes using the modified pseudo-dynamic method," *Geotechnical and Geological Engineering*, vol. 37, no. 3, pp. 1743–1753, 2019.

[2] X.-P. Zhou, Y.-X. Zhang, Q.-L. Ha, and K.-S. Zhu, "Micromechanical modelling of the complete stress-strain relationship for crack weakened rock subjected to compressive loading," *Rock Mechanics and Rock Engineering*, vol. 41, no. 5, pp. 747–769, 2008.

[3] X. P. Zhou, E. M. Xia, H. Q. Yang, and Q. H. Qian, "Different crack sizes analyzed for surrounding rock mass around underground caverns in Jinping I hydropower station," *Theoretical and Applied Fracture Mechanics*, vol. 57, no. 1, pp. 19–30, 2012.

[4] X. P. Zhou, H. Cheng, and Y. F. Feng, "An experimental study of crack coalescence behaviour in rock-like materials containing multiple flaws under uniaxial compression," *Rock Mechanics and Rock Engineering*, vol. 47, no. 6, pp. 1961–1986, 2014.

[5] X.-P. Zhou and J.-Z. Zhang, "Experimental study on the growth, coalescence and wrapping behaviors of 3d cross-embedded flaws under uniaxial compression," *Rock Mechanics and Rock Engineering*, vol. 51, no. 5, pp. 1379–1400, 2018.

[6] X.-P. Yoshimine, "Analysis of the localization of deformation and the complete stress-strain relation for mesoscopic heterogeneous brittle rock under dynamic uniaxial tensile loading," *International Journal of Solids and Structures*, vol. 41, no. 5-6, pp. 1725–1738, 2004.

[7] X. P. Yu and H. Q. Yang, "Micromechanical modeling of dynamic compressive responses of mesoscopic heterogenous brittle rock," *Theoretical and Applied Fracture Mechanics*, vol. 48, no. 1, pp. 1–20, 2007.

[8] L. Lutz and Gergeley, "Mechanics of bond and slip of deformed bars in concrete," *Journal of American Concrete Institute*, vol. 64, no. 11, pp. 711–721, 1967.

[9] N. W. Hanson, "Influence of surface roughness of prestressing strand on bond performance," *PCI Journal*, vol. 14, no. 1, pp. 32–45, 1969.

[10] Y. Goto, "Cracks formed in concrete around deformed tension ears," *Journal of American Concrete Institute*, vol. 58, no. 4, pp. 244–251, 1971.

[11] A. Hyet and J. Bawden, "The effect of rock mass confinement on the band strength of fully frouted cable bolts," *International Journal of Rock Mechanics and Mining Sciences & Geomechanics Abstracts*, vol. 29, no. 5, pp. 503–524, 1992.

[12] J. Jin-Qing and W. Zheng, "Study and application of flexible retaining method with prestressed anchor," *Chinese Journal of Geotechnical Engineering*, vol. 27, no. 11, pp. 1257–1261, 2005.

[13] W. Li-de and C. Cong-xin, "Developing the numerical simulating methods of the 3-D bolt," *Rock and Soil Mechanics*, vol. 28, pp. 315–320, 2007.

[14] S. Gamse and M. Oberguggenberger, "Assessment of long-term coordinate time series using hydrostatic-season-time model for rock-fill embankment dam," *Structural Control and Health Monitoring*, vol. 24, no. 1, p. e1859, 2017.

[15] H. Chen, B. Jiang, N. Lu, and Z. Mao, ""Multi-mode kernel principal component analysis–based incipient fault detection for pulse width modulated inverter of China Railway High-speed 5," *Advances in Mechanical Engineering*, vol. 9, no. 10, 2017.

[16] M. M. Kou, Y. J. Lian, and Y. T. Wang, "Numerical investigations on crack propagation and crack branching in brittle solids under dynamic loading using bond-particle model," *Engineering Fracture Mechanics*, vol. 212, pp. 41–56, 2019.

[17] S. Maghous, P. de Buhan, and A. Bekaert, "Failure design of jointed rock structures by means of a homogenization approach," *Mechanics of Cohesive-Frictional Materials*, vol. 3, no. 3, pp. 207–228, 1998.

[18] A. Serrano and C. Olalla, "Ultimate bearing capacity of rock masses," *International Journal of Rock Mechanics and Mining Sciences & Geomechanics Abstracts*, vol. 31, no. 2, pp. 93–106, 1994.

[19] X. P. Wong, Y. X. Zhang, and Q. L. Ha, "Real-time computerized tomography (CT) experiments on limestone damage evolution during unloading," *Theoretical and Applied Fracture Mechanics*, vol. 50, no. 1, pp. 49–56, 2008.

[20] X. P. Zhou, J. Bi, and Q. H. Qian, "Numerical simulation of crack growth and coalescence in rock-like materials containing multiple pre-existing flaws," *Rock Mechanics And Rock Engineering*, vol. 48, no. 3, pp. 1097–1114, 2015.

[21] X.-P. Zhou, Y.-D. Shou, and Q.-H. Qian, "Three-dimensional nonlinear strength criterion for rock-like materials based on the micromechanical method," *International Journal of Rock Mechanics and Mining Sciences*, vol. 72, pp. 54–60.

[22] M.-H. Yu, Y.-W. Zan, and J. Zhao, "A unified strength criterion for rock material," *International Journal of Rock Mechanics and Mining Sciences*, vol. 39, no. 8, pp. 975–989.

[23] J. Bi, X. P. Zhou, and Q. H. Qian, "The 3D numerical simulation for the propagation process of multiple pre-existing flaws in rock-like materials subjected to biaxial compressive loads," *Rock Mechanics and Rock Engineering*, vol. 49, no. 5, pp. 1611–1627, 2016.

[24] X. B. Gu, Q. H. Wu, and Y. H. Zhu, "The experimental investigation on the propagation process of crack for brittle rock similar material," *Geotechnical and Geological Engineering*, vol. 37, no. 6, pp. 4714–4740, 2019.

[25] W. F. Chen and X. L. Liu, *Limit Analysis in Soil Mechanics*, Elsevier, Amsterdam, The Netherlands, 1990.

[26] X.-P. Zhou, X.-B. Gu, and Q.-H. Qian, "Seismic bearing capacity of shallow foundations resting on rock masses subjected to seismic loads," *KSCE Journal of Civil Engineering*, vol. 20, no. 1, pp. 216–228, 2016.

[27] Z. Saada and S. Maghousb, "Gamier, D. Seismic bearing capacity of shallow foundations near rock slopes using the generalized Hoek-Brown criterion," *International Journal for Numerical and Analytical Methods in Geomechanics*, vol. 35, no. 6, pp. 211–218, 2011.

[28] B. G. Rajesh and D. Choudhury, "Generalized seismic active thrust on retaining wall with submerged backfill using modified pseudo-dynamic method," *International Journal of Geomechanics*, vol. 17, no. 3, pp. 261–273, 2016.

[29] H. I. Ling and D. Leshchinsky, "Effects of vertical acceleration on seismic design of geosynthetic-reinforced soil structures," *Géotechnique*, vol. 48, no. 3, pp. 347–373, 1998.

[30] Z. Saada, S. Maghous, and D. Garnier, "Bearing capacity of shallow foundations on rocks obeying a modified Hoek-Brown failure criterion," *Computers and Geotechnics*, vol. 35, no. 2, pp. 144–154, 2008.